

Supplementary Information

Large Variability and Complexity of Isothermal Solubility for a Series of Redox-Active Phenothiazines

Anton S. Perera,^{‡1,2,3} T. Malsha Suduwella,^{‡1,2} N. Harsha Attanayake,^{1,2} Rahul Kant Jha,¹ William L. Eubanks,¹ Ilya A. Shkrob,^{4,5} Chad Risko,^{*2,3} Aman Preet Kaur,^{*1,2} Susan A. Odom^{*1,2}

¹ Joint Center for Energy Storage Research, University of Kentucky, Lexington, KY 40506, USA

² Department of Chemistry, University of Kentucky, Lexington, KY 40506, USA

³ Center for Applied Energy Research, University of Kentucky, Lexington, KY 40511, USA

⁴ Joint Center for Energy Storage Research, Argonne National Laboratory, 9700 S. Cass Ave, Lemont, IL 60439, USA

⁵ Chemical Sciences and Engineering Division, Argonne National Laboratory, 9700 S. Cass Avenue, Lemont, Illinois, USA

[‡] The authors contributed equally to the manuscript.

Materials and Methods

Phenothiazine, sodium hydride (NaH, 60% dispersion in mineral oil) and Copper (I) iodide (98%), and propylene oxide were purchased from Acros Organics. *n*-BuLi, 2-chloroethylmethylether, NaH (95%), *N*-bromosuccinamide (NBS), sodium metal, anhydrous pyridine, and anhydrous methanol were purchased from Sigma Aldrich. 2-(trifluoromethyl)phenothiazine (2-CF₃PT), 1-bromo-2-(2-methoxyethoxy)ethane (MEEBr), *N*-methylphenothiazine (MPT), *N*-[2-(2-methoxyethoxy)ethyl]phenothiazine (MEEPT) and promethazine hydrochloride were purchased from TCI. Nitrosonium tetrafluoroborate (NOBF₄, 98%) was purchased from Alfa Aesar and was stored and weighed in an argon-filled glovebox (MBraun), and removed in a capped vial only immediately prior to use. Dry tetrahydrofuran (THF) was purchased from Fisher Chemicals and anhydrous *N,N'*-dimethylformamide (DMF) was purchased from Honeywell. Anhydrous magnesium sulfate, hexane, ethyl acetate, anhydrous diethyl ether and dichloromethane (DCM) were purchased from VWR. All reagents were used without further purification. Silica gel (65 x 250 mesh) was purchased from Sorbent Technologies. ¹H and ¹³C NMR spectra in DMSO-*d*₆ (Cambridge Isotope Laboratories) were obtained using a 400 MHz Bruker Avance NEO (equipped with a smart probe) NMR spectrometer. Mass spectra were obtained using an Agilent 5973 Network mass selective detector attached to an Agilent 6890N Network GC system.

Tetraethylammonium tetrafluoroborate (TEABF₄, 99.9%) was obtained from BASF. Acetonitrile (ACN, 99.9%) was purchased from Avantor (VWR) and dried using a solvent dispensing system (LC Technology Inc). Sodium thiosulfate pentahydrate (Na₂S₂O₃·5H₂O, 99%) was obtained from Beantown Chemical (VWR). ¹H NMR spectra for solubility determination were obtained on 400 MHz Bruker Avance NEO (equipped with a Smart Probe) with 1,4-bis(trifluoromethyl)benzene (>99%, TCI America) as an internal concentration standard in DMSO-*d*₆ (Cambridge Isotope Laboratories).

EPT,¹ PrPT,² *i*PrPT,³ BuPT,² *t*BuPT,³ HpPT,⁴ PhPT,³ BnPT,⁵ AcPT,⁶ BzPT,⁷ BOCPT,⁸ MEPT,¹ DCIEPT,⁹ DBrEPT,⁹ DBrMEEPT,¹⁰ DCNEPT,⁹ BCF₃EPT,¹¹ DMeOEPT,¹² DMeOMEPT,¹⁰ DMeOMEEPT,¹⁰ B(MEEO)EPT,¹⁰ 2-MeOEPT,¹³ and 10-(β-hydroxypropyl)phenothiazine¹⁴ were synthesized as previously reported. PRT was extracted from promethazine hydrochloride using reported procedure.¹⁵ All the tetrafluoroborate salts of phenothiazine derivatives (XPT-BF₄) were synthesized according to the general procedure published before.¹

Synthesis of N-(2-(2-methoxyethoxy)propyl)phenothiazine (Me-MEEPT)

In an oven-dried round bottom flask, 10-(β -hydroxypropyl)phenothiazine (6.00 g, 23.3 mmol) was dissolved in dry DMF (250 mL) at 0 °C and stirred using an oven dried stir bar. Sodium hydride, NaH (95%, 0.88 g, 35 mmol) was added in portions under nitrogen. After 45 min of stirring, 2-chloroethylmethyl ether (3.31 g, 3.50 mL, 35.0 mmol) was added dropwise over the period of 10 min. Then the reaction mixture was stirred for 15 min and refluxed overnight. Upon completion of the reaction, the reaction mixture was quenched by adding (60 g) of finely crushed ice, then extracted with diethyl ether. The combined organic layer was washed with brine, dried over anhydrous magnesium sulfate and concentrated under rotary evaporation. The crude product was purified by column chromatography using a 4:1 v/v mixture of hexanes and ethyl acetate (EtOAc) as an eluent to obtain product as pale yellow liquid (4.4 g, 60%). ¹H NMR (DMSO-d₆, 400 MHz, ppm) δ 7.16 – 7.23 (m, 4H) 7.08 – 7.10 (m, 2H), 6.94 – 6.98 (m, 2H), 3.99 – 4.05 (m, 1H), 3.78 – 3.83 (m, 2H), 3.50 – 3.59 (m, 2H), 3.31 – 3.38 (m, 2H), 3.17 (s, 3H), 1.15 (d, J = 5.81 Hz, 3H). ¹³C NMR (DMSO-d₆, 100 MHz, ppm) δ 145.6, 128.0, 127.7, 124.8, 123.1, 116.8, 72.6, 72.2, 68.4, 58.5, 52.9, 18.6. GCMS: m/z 315 (40%), 212 (100%), 198 (18%), 180 (37%).

Synthesis of N-ethyl-2-(trifluoromethyl)phenothiazine (2-CF₃EPT)

In an oven-dried 250 mL round-bottom flask, 2-(trifluoromethyl)phenothiazine (10.0 g, 37.4 mmol) was dissolved in dry DMF (100 mL) using an oven dried stir bar. Nitrogen was purged for 10 min. Then sodium hydride (60%, 1.80 g, 44.9 mmol) was added, allowing hydrogen to vent. Once bubbling stopped, bromoethane (4.89 g, 3.40 mL, 44.9 mmol) was added dropwise. A reflux condenser was attached, and the reaction was stirred 6 h at 50 °C or until thin layer chromatography (TLC) using 15 vol% EtOAc in hexanes as a mobile phase showed consumption of the starting material. The reaction mixture was quenched with ice water and vacuum filtered. The resulting solid was crystallized from ethanol to yield the title compound as a white solid (9.9 g, 90%). ¹H NMR (DMSO-d₆, 400 MHz, ppm) δ 7.33 – 7.35 (m, 1H) 7.21 – 7.26 (m, 2H), 7.15 – 7.17 (m, 2H), 6.97 – 7.06 (m, 2H), 3.97 (q, J = 6.92 Hz, 2H), 1.29 (t, J = 6.92 Hz, 3H). ¹³C NMR (DMSO-d₆, 100 MHz, ppm) δ 145.5, 144.0, 129.2, 129.0, 128.7, 128.5, 128.1, 127.7, 123.6, 122.6, 119.3, 116.5, 111.9, 41.7, 12.9. GCMS: m/z 295 (50%), 280 (13%), 266 (100%), 248 (9%).

Synthesis of 2-(trifluoromethyl)-N-(2-(2-methoxyethoxy)ethyl)phenothiazine (2-*CF*₃MEEPT)

2-(trifluoromethyl)phenothiazine (5.00 g, 19.0 mmol) was dissolved in 50 mL anhydrous DMF in a 250 mL round bottom flask containing stir bar. After purging nitrogen for 15 min, NaH (60%, 0.92 g, 23.0 mmol) was added allowing hydrogen gas to vent. After stirring 30 min at room temperature, 1-bromo-2-(2-methoxyethoxy)ethane (3.84 g, 2.90 mL, 21.0 mmol) was added. The reaction mixture was heated to 70 °C for 12 h. Upon completion of the reaction, the reaction mixture was quenched by adding ice water and extracted with EtOAc. The organic layer was washed with brine and dried over magnesium sulfate. The crude product was concentrated by rotary evaporation and purified by column chromatography using hexane as the eluent to obtain product as pale yellow liquid (5.7 g, 83%). ¹H NMR (DMSO-*d*₆, 400 MHz, ppm) δ 7.33 – 7.34 (m, 2H), 7.15 – 7.27 (m, 3H), 6.97 – 7.06 (m, 2H), 4.11 (t, J = 5.48 Hz, 2H), 3.76 (t, J = 5.48 Hz, 2H), 3.52 – 3.54 (m, 2H), 3.40 – 3.42 (m, 2H), 3.20 (s, 3H). ¹³C NMR (DMSO-*d*₆, 100 MHz, ppm) δ 145.6, 144.2, 129.3, 129.0, 128.7, 128.5, 128.1, 127.7, 123.7, 122.7, 119.5, 116.6, 112.5, 71.7, 70.2, 68.1, 58.5, 48.0. GCMS: m/z 369 (49%), 280 (100%), 266 (21%), 248 (49%).

Synthesis of 3-bromo-N-ethylphenothiazine (3-BrEPT)

To a solution of *N*-ethylphenothiazine (7.41 g, 32.6 mmol) in DMF (32 mL) in a round bottomed flask, freshly recrystallized *N*-bromosuccinimide (5.80 g, 32.6 mmol) in DMF (32 mL) was added dropwise at 0 °C, and the reaction mixture was stirred at 0 °C for 4 hours and let warm up at room temperature overnight. Upon completion, water (60 mL) and brine (60 mL) were added to the reaction mixture followed by saturated aqueous sodium thiosulfate (15 mL), and the organic product was extracted with DCM (3 x 50 mL). The combined organic layers were dried over magnesium sulfate and concentrated by rotary evaporation. The crude product was purified by column chromatography (hexane/EtOAc, 19:1 to 9:1), yielding the product as a yellow solid (8.1 g, 81%). ¹H NMR (DMSO-*d*₆, 400 MHz, ppm) δ 7.32 – 7.35 (m, 2H), 7.13 – 7.23 (m, 2H), 6.92 – 7.03 (m, 3H), 3.88 (q, J = 6.92 Hz, 2H), 1.28 (t, J = 6.92 Hz, 3H). ¹³C NMR (DMSO-*d*₆, 100 MHz, ppm) δ 144.5, 144.3, 130.6, 129.3, 128.4, 127.6, 126.1, 123.2, 122.7, 117.5, 116.1, 114.1, 41.7, 13.0. GCMS: m/z 306 (50%), 305 (50%), 278 (100%), 276 (100%), 196 (28%), 153 (12%).

Synthesis of *N*-ethyl-3-methoxy-phenothiazine (3-MeOEPT)

In a 250 mL round-bottomed flask immersed in an ice-water bath, a 5 M solution of sodium methoxide was prepared by dissolving sodium (2.23 g, 97.2 mmol) in methanol (17.40 mL) under nitrogen atmosphere. To the resultant solution, copper(I) iodide (7.40 g, 38.86 mmol), 3-bromo-*N*-ethylphenothiazine (5.95 g, 19.4 mmol), and anhydrous pyridine (43.5 mL) were added. The reaction mixture was sparged with nitrogen for 15 min. A reflux condenser was attached, and the reaction was heated at reflux for 12 h. Upon completion, the reaction mixture was diluted with brine (50 mL), and the aqueous phase was extracted with diethyl ether (3 x 50 mL). The organic solution was dried over magnesium sulfate, filtered to remove solids, and concentrated by rotary evaporation. The organic residue was purified by column chromatography to obtain a white crystalline solid (3.5 g, 70%). ¹H NMR (DMSO-*d*₆, 400 MHz, ppm) δ 7.12 – 7.20 (m, 2H) 6.77 – 6.98 (m, 5H), 3.86 (q, *J* = 6.88 Hz, 2H), 3.70 (s, 3H), 1.27 (t, *J* = 6.88 Hz, 3H). ¹³C NMR (DMSO-*d*₆, 100 MHz, ppm) δ 155.4, 145.5, 138.2, 128.1, 127.4, 125.1, 123.2, 122.3, 116.6, 115.6, 113.4, 112.9, 55.9, 41.6, 13.2. GCMS: *m/z* 257 (47%), 242 (4%), 228 (100%), 185 (25%).

Solubility Determination Using ¹H NMR Spectroscopy

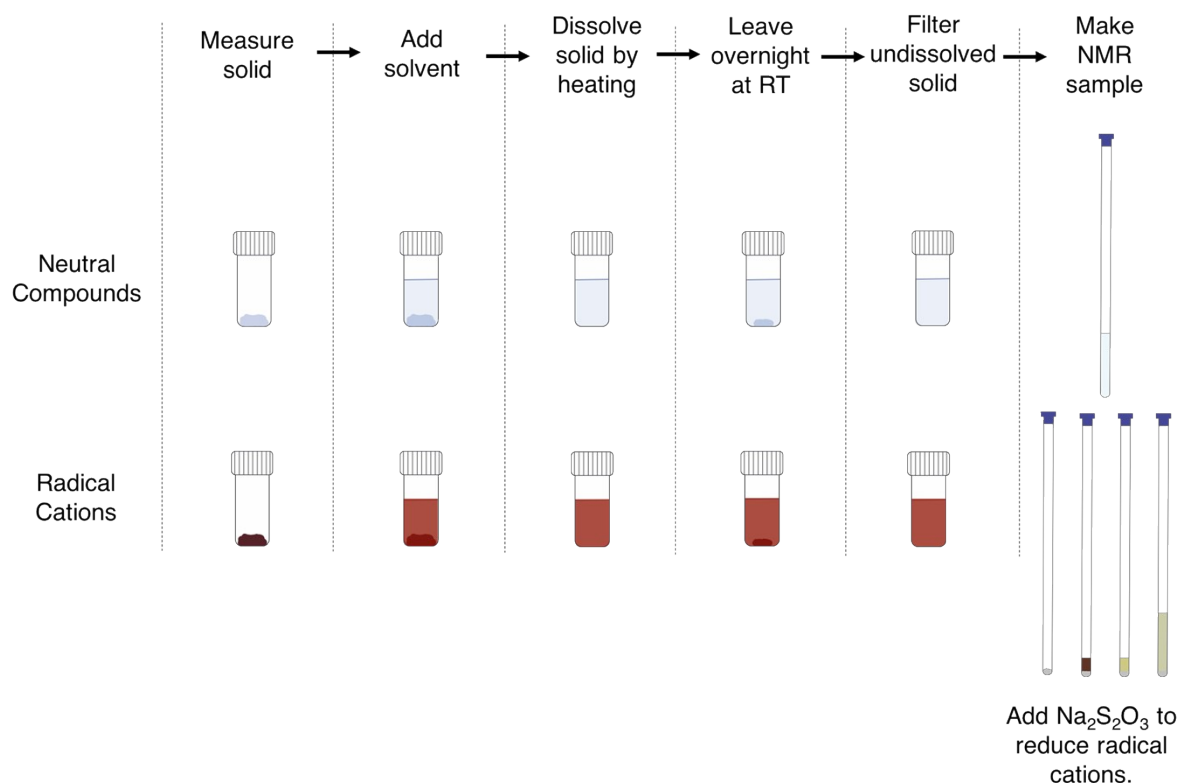


Figure S1. Schematic diagram for solubility determination using ¹H NMR spectroscopy.

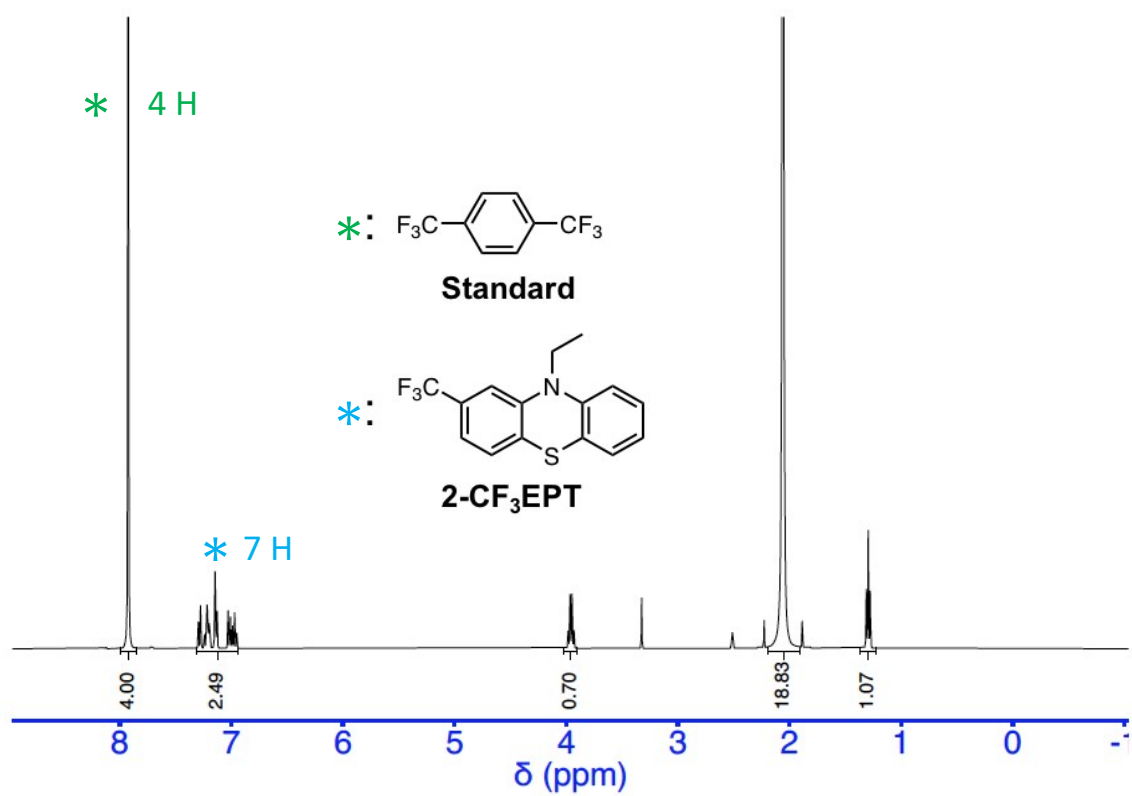
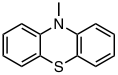
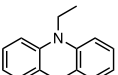
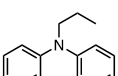
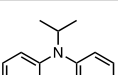
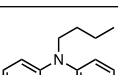
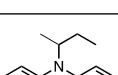
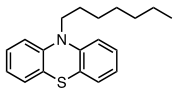
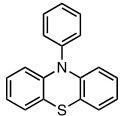
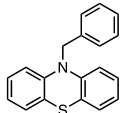
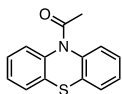
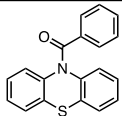
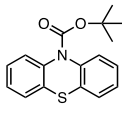
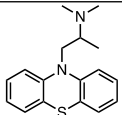
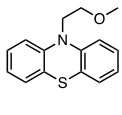
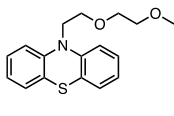
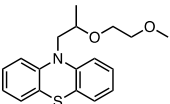
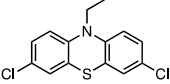
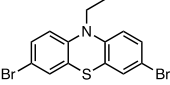
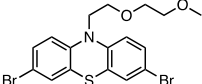
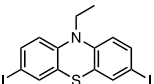
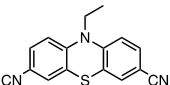
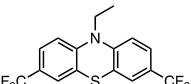


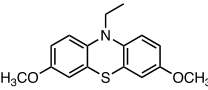
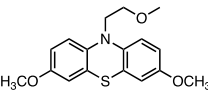
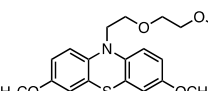
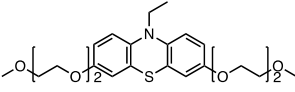
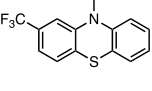
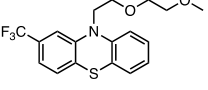
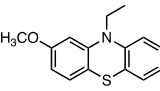
Figure S2. The proton NMR spectrum of the 2-CF₃EPT saturated solution (120 μ L) in the presence of the internal standard (1,4-bis(trifluoromethyl)benzene) in DMSO-*d*₆ (120 μ L).

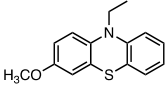
Table S1. PT solubilities (molarity at saturation at 298 K) in the neutral state and radical-cation states with the structure of the molecule, name, and molecular weight, MW. (N/A: solubility could not be determined as the radical-cation salts were unstable).

Structure	Name (abbreviation)	MW (g/mol)	Solubility (M)			
			Neutral		Radical cation salt	
			ACN	0.5 M TEABF ₄ in ACN	ACN	0.5 M TEABF ₄ in ACN
	<i>N</i> -methylphenothiazine MPT	213.30	0.239	0.263	0.710	0.489
	<i>N</i> -ethylphenothiazine EPT	227.33	0.113	0.113	0.281	0.179
	<i>N</i> -propylphenothiazine PrPT	241.35	m	0.60	0.192	0.107
	<i>N-iso</i> -propylphenothiazine iPrPT	241.35	0.345	0.315	0.528	0.278
	<i>N</i> -butylphenothiazine BuPT	255.38	m	1.26	0.506	0.354
	<i>sec</i> -butylphenothiazine sec-BuPT	255.38	0.44	0.40	0.60	0.50
	<i>N-(tert-</i> butyl)phenothiazine tBuPT	255.38	0.055	0.048	N/A	N/A

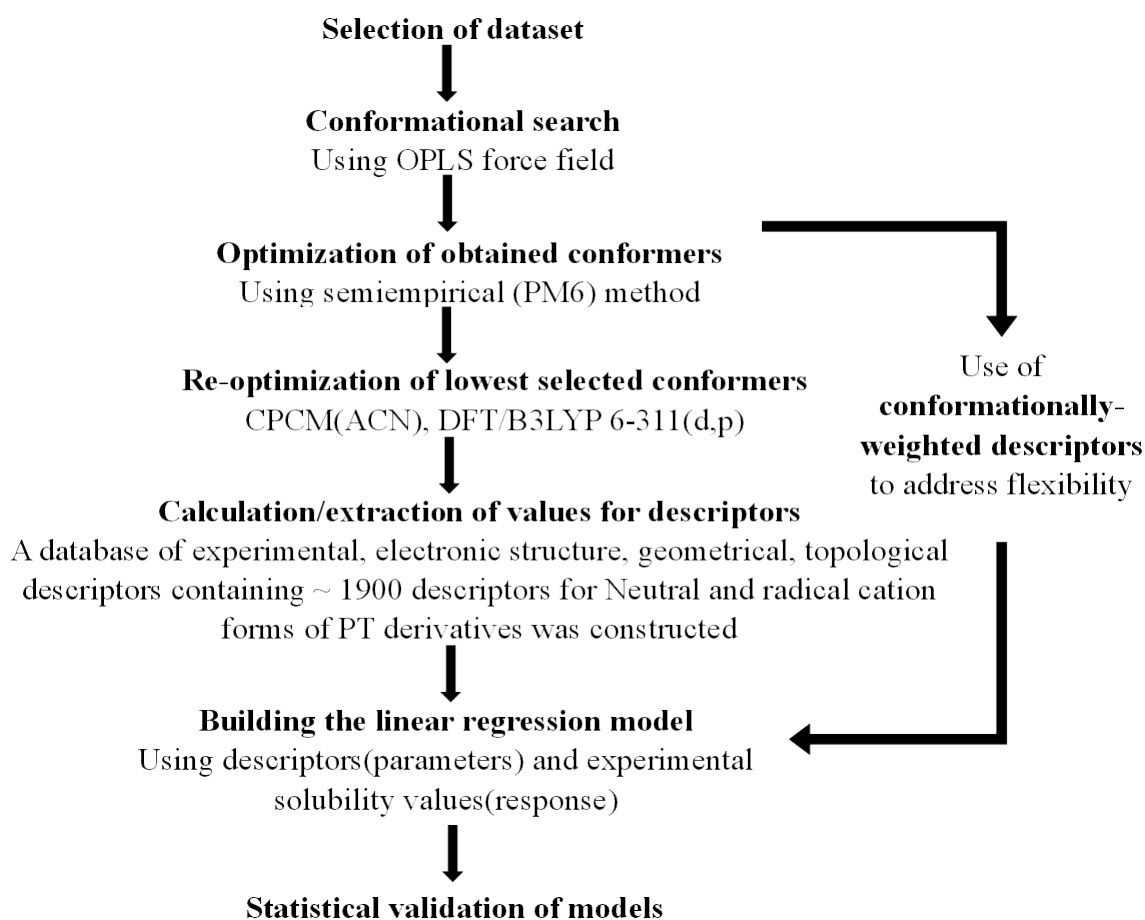
	<i>N</i> -heptylphenothiazine HpPT	297.46	0.402	0.286	0.574	0.429
	<i>N</i> -phenylphenothiazine PhPT	275.37	0.139	0.126	0.603	0.480
	<i>N</i> -benzylphenothiazine BnPT	289.40	0.150	0.131	0.097	0.044
	<i>N</i> -acetylphenothiazine AcPT	241.31	0.0215	0.0216	N/A	N/A
	<i>N</i> -benzoylphenothiazine BzPT	303.38	0.0711	0.0707	N/A	N/A
	<i>N</i> - (methylcarbamate)phenot hiazine BOCPT	299.39	0.162	0.142	N/A	N/A
	Promethazine PRT	284.42	2.39	1.10	N/A	N/A
	<i>N</i> -(2- methoxyethyl)phenothiazine MEPT	257.35	3.45	3.58	0.318	0.224
	<i>N</i> -(2-(2- methoxyethoxy)ethyl)phe nothiazine MEEPT	301.40	m	m	0.553	0.453

	<i>N</i> -(1-methyl-(2-(2-methoxyethoxy)ethyl)phenothiazine Me-MEEPT	315.43	m	m	0.526	0.390
	3,7-dichloro- <i>N</i> -ethylphenothiazine DCIEPT	296.21	0.183	0.173	0.087	0.058
	3,7-dibromo- <i>N</i> -ethylphenothiazine DBrEPT	385.12	0.058	0.060	0.075	0.045
	3,7-dibromo- <i>N</i> -(2-(2-methoxyethoxy)ethyl)phenothiazine DBrMEEPT	459.20	0.598	0.390	0.178	0.0988
	<i>N</i> -ethyl-3,7-diiodophenothiazine DIEPT	479.12	0.0135	0.0131	N/A	N/A
	3,7-dicyano- <i>N</i> -ethylphenothiazine DCNEPT	277.35	0.0146	0.0134	N/A	N/A
	<i>N</i> -ethyl-3,7-bis(trifluoromethyl)phenothiazine BCF₃EPT	363.32	m	m	0.349	0.250

	<i>N</i> -ethyl-3,7-dimethoxyphenothiazine DMeOEPT	287.38	0.059	0.059	0.062	0.046
	3,7-dimethoxy- <i>N</i> -(2-methoxyethyl)phenothiazine DMeOMEPT	317.40	0.241	0.223	0.137	0.137
	3,7-dimethoxy- <i>N</i> -(2-(2-methoxyethoxy)ethyl)phenothiazine DMeOMEEPT	361.46	m	m	0.183	0.085
	<i>N</i> -ethyl-(3,7-bis(2-(2-methoxyethoxy)ethoxy)phenothiazine B(MEEO)EPT	463.59	m	m	0.77	0.63
	<i>N</i> -ethyl-2-(trifluoromethyl)phenothiazine 2-CF₃EPT	295.32	0.96	0.68	0.230	0.210
	2-(trifluoromethyl)- <i>N</i> -(2-(2-methoxyethoxy)ethyl)phenothiazine 2-CF₃MEEPT	369.40	m	m	0.18	0.172
	<i>N</i> -ethyl-2-methoxyphenothiazine	257.35	0.138	0.134	N/A	N/A

	2-MeOEPT					
	<i>N</i> -ethyl-3-methoxy- phenothiazine 3-MeOEPT	257.35	0.225	0.194	N/A	N/A

Computational and MLR details



Schematic S1. Computational workflow used for descriptor generation. For the descriptor calculations: i) the estimates of the butterfly angles were obtained using DFT optimized geometry using Mercury crystallography analysis package;¹⁶ the SASA calculations were carried out using the PyMol package;¹⁷ and, iii) for the the weighted sterimol descriptor, the temperature for the Boltzman distribution was set to 298 K and the energy cutoff for conformers was 20.9 kJ/mol. All these calculations were automated with the wSterimol python package.¹⁸

The molecule descriptors were computed using the optimized geometry parameters obtained from the DFT calculations as described in the Methods section. A set of 3D descriptors that were extracted from DFT calculations of the lowest energy conformers of selected PT were included in the database of molecular descriptors. Although the use of DFT-based descriptors is somewhat discouraged in the chemistry data science community due to the high computational cost when creating large databases, we hypothesized that electronic structure

properties particularly related to molecular charges would be important in addressing these systems (specifically the radical cation salts). There is no guarantee that only the descriptors that we would include in the descriptor library using our chemical intuition would work, owing to fairly complex structure of these derivatives. So, we added as many descriptors as possible assuming that the model search would be able to select the most appropriate ones. Mordred is a free use Python package that enabled us to generate more than 1800 descriptors for each neutral PT molecule. There are 48 basic categories, and in each category there are descriptors with slight differences. These descriptors consist of 1D, 2D, and 3D descriptors that cover a vast area of search space. A complete table of the different types can be found in Table 3 of the original publication by Moriwaki *et. al.*¹⁹

A molecular-descriptor-calculation software such as Mordred generates a large set of data that is tedious to process manually. Furthermore performing multiple linear regression (MLR) for such a database is computationally expensive. Therefore, the descriptor set was refined and reduced. We developed an in-house Python script that generates descriptors, cleans, filters and provides an output as a spreadsheet that can be used in the MLR computation. The basic script workflows follows: i) import molecules in mol format into RDkit chem module²⁰ – this allows us to use 3D quantum-mechanically optimized molecular structures, which differ from 2D SMILES inputs; ii) call Mordred to generate 1825 descriptors, including 214 3D descriptors;²¹ iii) remove descriptors without values; iv) perform an (optional) principal component analysis to reduce the number of descriptors to 30; v) remove highly correlated (Pearson’s correlation coefficient > 0.9) descriptors (from step iii) to reduce the dimensionality; vi) remove descriptors with constant (variance threshold > 0.9) values for all molecules.

The down selection process was comprised of both automated steps coupled with human intervention. The automation followed the following steps as further described in Guo *et al.*:²²

- a) Models whose $R^2 < Q^2$ (to remove models with leave-one-out predictions that could line up by chance yet be far-off from the real fit line) were removed
- b) The R^2 , Q^2 , validation R^2 , wholeset R^2 , and k-fold R^2 values were normalized; thus from the remainder, all models that had negative values for the normalized statistics were removed.
- c) From the remaining models, the weighted wholeset R^2 (wR^2_{\max}) from the best validated model (with the highest validation R^2); subsequently all models that had wholeset $R^2 < (wR^2_{\max} - 0.3)$ were removed.

d) Models with strong descriptor intercorrelations were removed.

This process yielded a set of models that was subjected to human arbitration, which included visual inspection of the model outputs and prediction accuracy of the validation data points considering the significance of the molecules that would best validate the model and which were expected to be predicted better based on prior intuition. Upon the examination of these models, it was evident that the lowest number of descriptors that could pass through the above selection was four. We removed models that used more than six descriptors since with our data set of limited data points that can be used (18 for radical cation systems), a number of descriptors higher than six could strongly suggest an overfit. Thus the models we ended up with after initial benchmark included four-to-six descriptors, with the highest percentage of models having five descriptors. Likewise, the neutral systems were allowed up to seven descriptors given that the number of data points available for modeling is 22. (These data sets are available in Supplementary Information).

The models that are reported in the main text represent the models with closest numerical prediction of *sec*-butyl-PT solubility and the set of models reported in SI are the ones that have high R^2 , Q^2 and wholset R^2 for each system. However, other down-selected models for which model data is available in the Supplementary Information show comparable results, though they are not presented graphically in the paper.

With the MLR, we seek approximate solutions

$$solubility = a_i \times descriptor1 + b_i \times descriptor2 + \dots$$

for each molecule I ; the linear coefficients (a_i, b_i, \dots) are different for different compounds (data points).

As noted in the main text, the down-selection process ultimately resulted in seven models for neutral PT and ten models for radical-cation PT. (All model information is provided in supplementary files.) Figure S3 (a) presents a predictive model with four different descriptors and five variables with one variable being a cross term of two descriptors that are already in the model. It can be described with the equation (note that the coefficients are mere averages),

$$solubility = 0.222 + 0.095 * Schr + 0.072 * RP + 0.241 * SsssN - 0.032 * ZMIC - 0.083Schr * ZMIC$$

where

- Schr is the Mulliken partial charge on S atom,
- RP is redox potential estimated using DFT calculations,
- SsssN is a descriptor named sum of sssN (is the sum of electro-topological state indices that corresponds to a N atom with three sigma bonds (as in the N on the PT core)).²³⁻²⁴
- ZMIC3 another descriptor named 3-ordered Z-modified information content describes the neighborhood (topologically connected map of atoms) symmetry of the molecule.²⁵⁻

26

Figure S3 (b) represents a predictive model with 6 different descriptors and 7 variables with the equation,

$$solubility = 0.24 - 0.21 * Cv + 0.62 * S + 0.17 * Schr - 0.31 * SASA(ACN) - 0.06 * ATSC7p + 0.23 * SsssN$$

where

- Cv is calculated heat capacity,
- S is the configurational entropy,
- SASA(ACN) is the solvent accessible surface area with respect to ACN,
- ATSC7p is the centered Moreau-Broto autocorrelation of lag 7 weighted by polarizability and the rest have the same meaning as defined above.

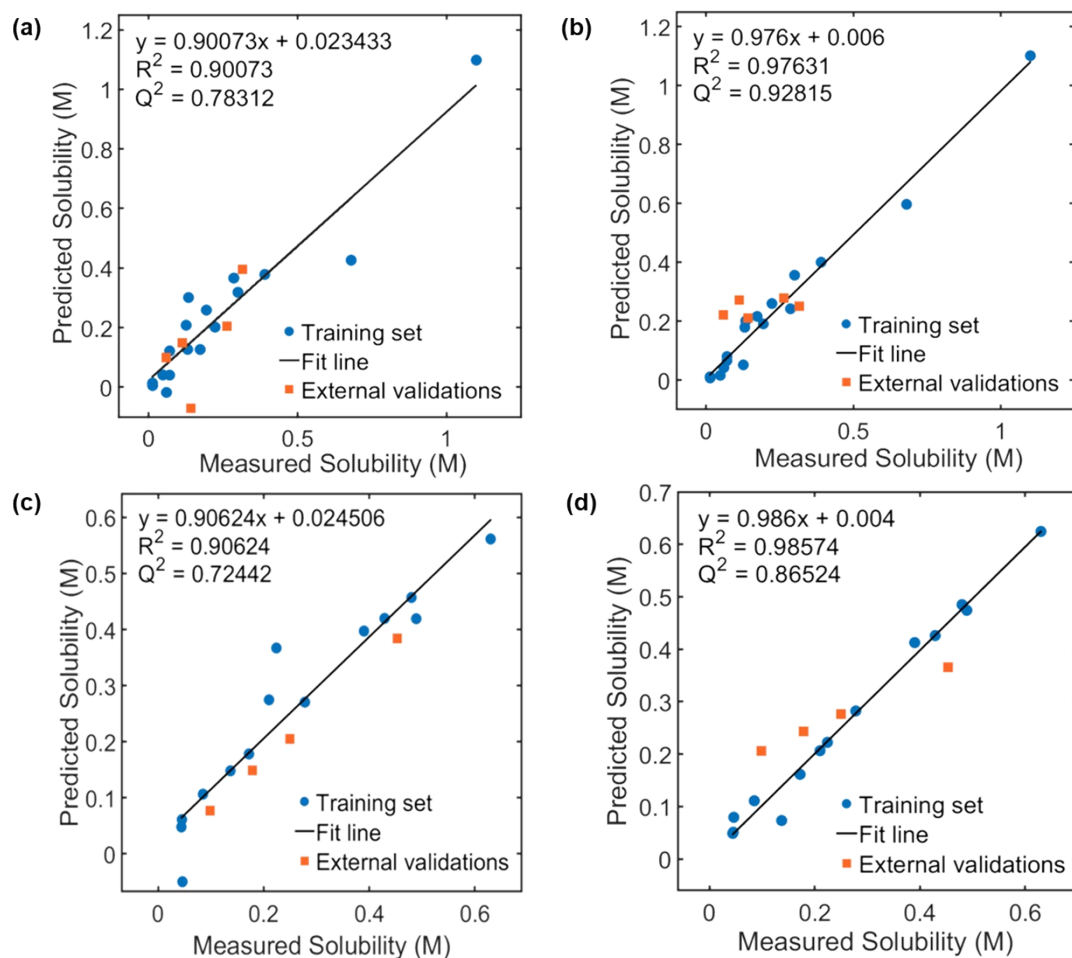


Figure S3. Predictive models for PT neutral states with (a) four and (b) six descriptors and for the radical-cation states with (c) four and (d) six descriptors.

Both of these models have a reasonably good level of statistical accuracy. However, most of the data points are clustered in the solubility region of 0 to 0.4 M, which would have a detrimental effect on the overall accuracy and the precision of all models for neutral PT.

Figure S3 (c) and (d) corresponds to predictive models of radical-cation systems. Figure S3 (c) represents a predictive model with four different descriptors and five variables with one variable being a cross term of two descriptors that are already in the model. The predicted solubility can thus be expressed as,

$$\begin{aligned} \text{Solubility} &= 0.26 + 0.09 * AATS7i - 0.16 * ATSC2Z + 0.17 * ATSC4v - 0.06 * ATSC3p - 0.17 \\ & * AATS7i * ATSC3p \end{aligned}$$

where

- AATS7i is the averaged moreau-broto autocorrelation of lag 7 weighted by ionization potential,
- ATSC2Z is the centered moreau-broto autocorrelation of lag 2 weighted by atomic number,
- ATSC4v is the centered moreau-broto autocorrelation of lag 4 weighted by the van der Waals (VdW) volume,
- ATSC3p is the centered moreau-broto autocorrelation of lag 3 weighted by polarizability.²⁷⁻³⁰

Figure S3 (d) presents a model with six different descriptors and seven variables with one variable being a cross term of two descriptors that are already in the model with the equation,

$$\begin{aligned} \text{solubility} &= 0.206 - 0.02 * ABC - 0.11 * VR1a - 0.09 * ATSC1d + 0.17 * ATSC4v + 0.40 * PEOE_VSA9 \\ &- 0.26 * MOMIZ + 0.10 * ABC * MOMIZ \end{aligned}$$

where

- ABC is atom-bond connectivity index,
- VR1a is a topological descriptor that represents a set of connections between adjacent pairs of atoms,
- ATSC1d is centered moreau-broto autocorrelation of lag 1 weighted by sigma electrons,
- PEOE_VSA9 is a descriptor that describes MOE-partialcharges and surface area contributions,
- MOMIZ is the moment of inertia around the (long) z-axis.

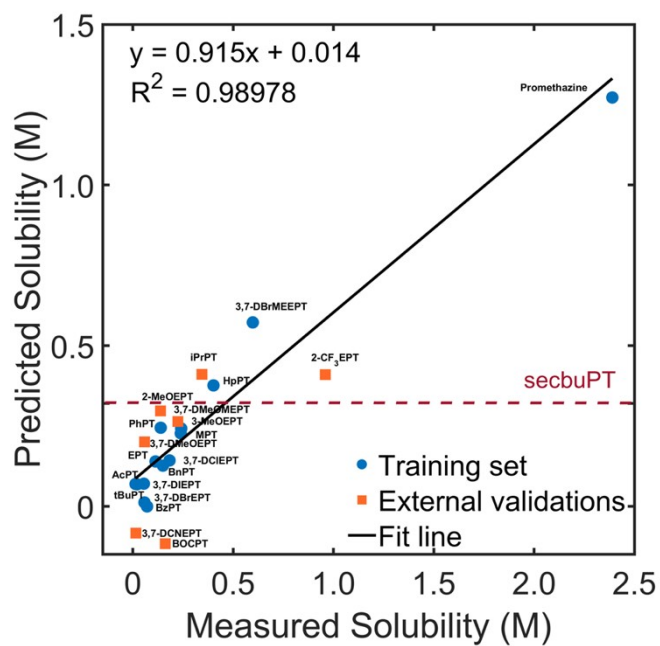


Figure S4. Model for the solubility of *sec*-butylPT in ACN.

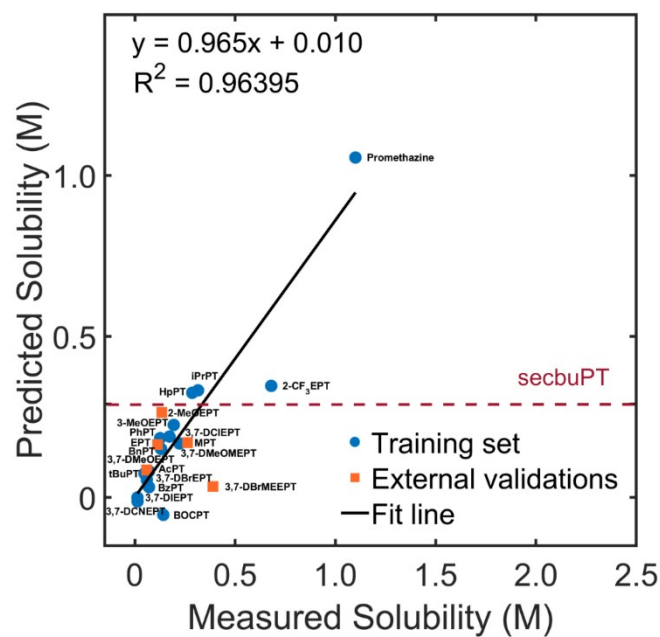


Figure S5. Model for solubility of *sec*-butylPT in 0.5 M TEABF₄ in ACN.

Through this process, it was observed that the fit was not significantly affected by this change when R^2 values are considered. The predicted solubility of sec-butylPT changed from 0.32 M to 0.34 M (vs 0.44 M, experimental) for ACN and 0.29 M to 0.23 M (vs 0.40 M, experimental) for 0.5 M TEABF₄ in ACN upon thinning out data points within 0-0.5 M.

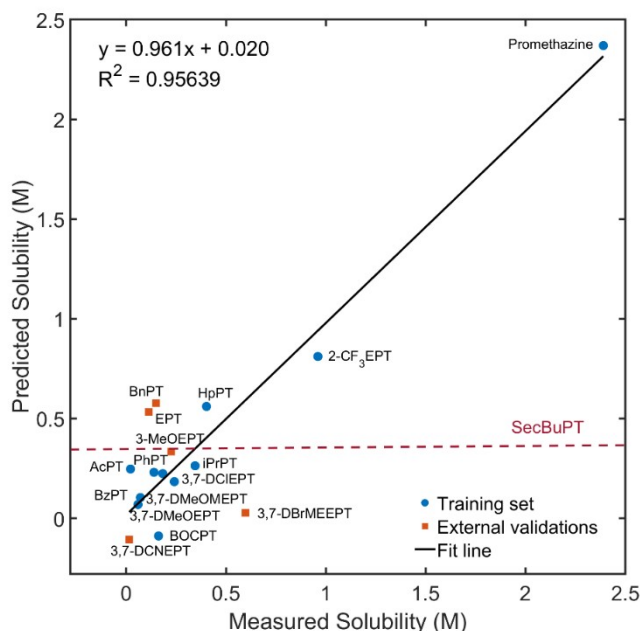


Figure S8. Model for the solubility of sec-butylPT in ACN (thinned out).

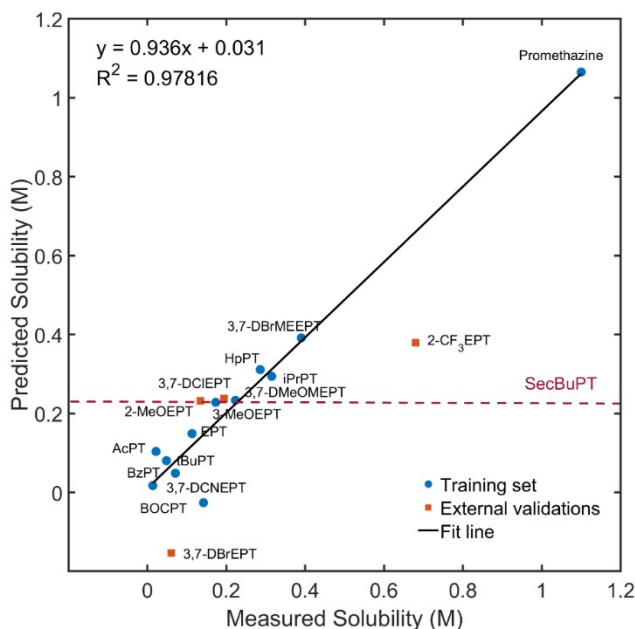


Figure S9. Model for solubility of sec-butylPT in 0.5 M TEABF₄ in ACN (thinned out).

Supporting References

1. Milshtein, J. D.; Kaur, A. P.; Casselman, M. D.; Kowalski, J. A.; Modekrutti, S.; Zhang, P. L.; Attanayake, N. H.; Elliott, C. F.; Parkin, S. R.; Risko, C.; Brushett, F. R.; Odom, S. A., High Current Density, Long Duration Cycling of Soluble Organic Active Species for Non-Aqueous Redox Flow Batteries. *Energy Environ. Sci.* **2016**, *9*, 3531-3543.
2. Darling, R. M.; Gallagher, K. G.; Kowalski, J. A.; Ha, S.; Brushett, F. R., Pathways to Low-Cost Electrochemical Energy Storage: A Comparison of Aqueous and Nonaqueous Flow Batteries. *Energy Environ. Sci.* **2014**, *7*, 3459-3477.
3. Narayana, K. A.; Casselman, M. D.; Elliott, C. F.; Ergun, S.; Parkin, S. R.; Risko, C.; Odom, S. A., N-Substituted Phenothiazine Derivatives: How the Stability of the Neutral and Radical Cation Forms Affects Overcharge Performance in Lithium-Ion Batteries. *ChemPhysChem* **2015**, *16* (6), 1179-1189.
4. Rajakumar, P.; Kanagalatha, R., Synthesis and optoelectrochemical properties of novel phenothiazinophanes. *Tetrahedron Lett.* **2007**, *48* (48), 8496-8500.
5. Sun, D.; Rosokha, S. V.; Kochi, J. K., Donor–Acceptor (Electronic) Coupling in the Precursor Complex to Organic Electron Transfer: Intermolecular and Intramolecular Self-Exchange between Phenothiazine Redox Centers. *Journal of the American Chemical Society* **2004**, *126* (5), 1388-1401.
6. Auvin, S.; Chabrier, d. L. P.-E. Preparation of 2-hydroxytetrahydrofuran peptide derivatives for use as medicaments. US7384933B2, 2008.
7. Tian, S.; Ma, H.; Wang, X.; Lv, A.; Shi, H.; Geng, Y.; Li, J.; Liang, F.; Su, Z. M.; An, Z., Utilizing d– π bonds for ultralong organic phosphorescence. *Angew. Chem. Int. Ed.* **2019**, *58* (20), 6645-6649.
8. Darvesh, S.; Darvesh, K. V.; McDonald, R. S.; Mataija, D.; Walsh, R.; Mothana, S.; Lockridge, O.; Martin, E., Carbamates with differential mechanism of inhibition toward acetylcholinesterase and butyrylcholinesterase. *J. Med. Chem.* **2008**, *51* (14), 4200-4212.
9. Ergun, S.; Elliott, C. F.; Kaur, A. P.; Parkin, S. R.; Odom, S. A., Overcharge performance of 3,7-disubstituted N-ethylphenothiazine derivatives in lithium-ion batteries. *Chem. Comm.* **2014**, *50* (40), 5339-5341.
10. Attanayake, N. H.; Kowalski, J. A.; Greco, K.; Casselman, M. D.; Milshtein, J. D.; Chapman, S. J.; Parkin, S. R.; Brushett, F. R.; Odom, S. A., Tailoring Two-Electron Donating Phenothiazines to Enable High Concentration Redox Electrolytes for Use in Nonaqueous Redox Flow Batteries. *Chem. Mater.* **2019**, *31*, 4353-4363.
11. Ergun, S.; Casselman, M. D.; Kaur, A. P.; Attanayake, N. H.; Parkin, S. R.; Odom, S. A., Improved synthesis of N-ethyl-3,7-bis(trifluoromethyl)phenothiazine. *New J. Chem.* **2020**, *44* (26), 11349-11355.
12. Kowalski, J. A.; Casselman, M. D.; Kaur, A. P.; Milshtein, J. D.; Elliott, C. F.; Modekrutti, S.; Attanayake, N. H.; Zhang, N.; Parkin, S. R.; Risko, C.; Brushett, F. R.; Odom, S. A., A Stable Two-Electron-Donating Phenothiazine for Application in Nonaqueous Redox Flow Batteries. *J. Mater. Chem. A* **2017**, *5*, 24371-24379.
13. Hou, J.-T.; Wang, B.; Zhang, Y.; Cui, B.; Cao, X.; Zhang, M.; Ye, Y.; Wang, S., Observation of peroxyxynitrite overproduction in cells during 5-fluorouracil treatment via a ratiometric fluorescent probe. *Chem. Comm.* **2020**, *56* (18), 2759-2762.
14. Borowiecki, P.; Paprocki, D.; Dranka, M., First chemoenzymatic stereodivergent synthesis of both enantiomers of promethazine and ethopropazine. *Beilstein Journal of Organic Chemistry* **2014**, *10*, 3038-3055.
15. Bate, A. B.; Kalin, J. H.; Fooksman, E. M.; Amorose, E. L.; Price, C. M.; Williams, H. M.; Rodig, M. J.; Mitchell, M. O.; Cho, S. H.; Wang, Y.; Franzblau, S. G., Synthesis and

antitubercular activity of quaternized promazine and promethazine derivatives. *Bioorganic & Medicinal Chemistry Letters* **2007**, *17* (5), 1346-1348.

16. Macrae, C. F.; Sovago, I.; Cottrell, S. J.; Galek, P. T. A.; McCabe, P.; Pidcock, E.; Platings, M.; Shields, G. P.; Stevens, J. S.; Towler, M.; Wood, P. A., Mercury 4.0: from visualization to analysis, design and prediction. *J Appl Crystallogr* **2020**, *53* (Pt 1), 226-235.

17. DeLano, W. L., PyMOL. 2002.

18. Brethomé, A. V.; Fletcher, S. P.; Paton, R. S., Conformational Effects on Physical-Organic Descriptors: The Case of Sterimol Steric Parameters. *ACS Catalysis* **2019**, *9* (3), 2313-2323.

19. Moriwaki, H.; Tian, Y.-S.; Kawashita, N.; Takagi, T., Mordred: a molecular descriptor calculator. *Journal of Cheminformatics* **2018**, *10* (1).

20. Landrum, G., RDKit: A software suite for cheminformatics, computational chemistry, and predictive modeling. Academic Press: 2013.

21. Moriwaki, H.; Tian, Y. S.; Kawashita, N.; Takagi, T., Mordred: a molecular descriptor calculator. *J Cheminform* **2018**, *10* (1), 4.

22. Guo, J.-Y.; Minko, Y.; Santiago, C. B.; Sigman, M. S., Developing Comprehensive Computational Parameter Sets To Describe the Performance of Pyridine-Oxazoline and Related Ligands. *ACS Catalysis* **2017**, *7* (6), 4144-4151.

23. Kier, L. B.; Hall, L. H., An electrotopological-state index for atoms in molecules. *Pharm Res* **1990**, *7* (8), 801-7.

24. Kier, L. B.; Hall, L. H., *Pharmaceutical Research* **1990**, *07* (8), 801-807.

25. Basak, S. C.; Magnuson, V. R.; Niemi, G. J.; Regal, R. R., Determining structural similarity of chemicals using graph-theoretic indices. *Discrete Applied Mathematics* **1988**, *19* (1-3), 17-44.

26. Basak, S. C.; Magnuson, V. R.; Niemi, G. J.; Regal, R. R.; Veith, G. D., Topological indices: their nature, mutual relatedness, and applications. *Mathematical Modelling* **1987**, *8*, 300-305.

27. Hollas, B., An Analysis of the Autocorrelation Descriptor for Molecules. *Journal of Mathematical Chemistry* **2003**, *33* (2), 91-101.

28. Moreau, G., The autocorrelation of a topological structure: A new molecular descriptor. **1980**.

29. Molecular structures perception auto correlation descriptor and structure activity relationship studies auto correlation descriptor. *European Journal of Medicinal Chemistry* **1984**, *19* (1), 66-70.

30. Devillers, J.; Balaban, A. T., *Topological Indices and Related Descriptors in QSAR and QSPAR*. Taylor & Francis: 2000.